Cross-shell excitations in ^{31}Si

P.-L. Tai, S. L. Tabor, R. S. Lubna, K. Kravvaris, P. C. Bender, Vandana Tripathi, A. Volya, M. P. Carpenter, R. V. F. Janssens, T. Lauritsen, E. A. McCutchan, S. Zhu, R. M. Clark, P. Fallon, S. Paschalis, M. Petri, A. O. Macchiavelli, W. Reviol, and D. G. Sarantites

Phys. Rev. C **96**, 014323 — Published 28 July 2017

DOI: 10.1103/PhysRevC.96.014323

Cross-shell excitations in ^{31}Si

P.-L. Tai, S. L. Tabor, R. S. Lubna, K.Kravvaris,

P. C. Bender, Vandana Tripathi, and A.Volya

Department of Physics, Florida State University, Tallahassee, Florida 32306, USA

M.P. Carpenter, R.V.F. Janssens, T. Lauritsen, E. A. McCutchan, and S. Zhu

Argonne National Laboratory, Argonne, Illinois, 60439, USA

R. M. Clark, P. Fallon, S. Paschalis, M. Petri, and A. O. Macchiavelli

Lawrence Berkeley National Laboratory, Berkeley, California 94720

W. Reviol and D.G. Sarantites

Washington University, St. Louis, Missouri 63130, USA

(Dated: June 29, 2017)

Abstract

The ^{31}Si nucleus was produced through the ^{18}O(^{18}O, αn) fusion-evaporation reaction at E_{lab} = 24 MeV. Evaporated α particles from the reaction were detected and identified in the Microball detector array for channel selection. Multiple γ-ray coincidence events were detected in Gammasphere. The energy and angle information for the α particles was used to determine the ^{31}Si recoil kinematics on an event-by-event basis for a more accurate Doppler correction. A total of 22 new states and 52 new γ transitions were observed, including 14 from states above the neutron separation energy. The positive-parity states predicted by the shell-model calculations in the *sd* model space agree well with experiment. The negative-parity states were compared with shell-model calculations in the *psdpf* model space with some variations in the $N = 20$ shell gap. The best agreement was found with a shell gap intermediate between that originally used for $A \approx 20$ nuclei and that previously adapted for ^{32,34}P. This variation suggests the need for a more universal cross-shell interaction.

I. INTRODUCTION

The ^{31}Si nucleus has long presented an excellent test case for study of the structure of a nucleus near the middle of the *sd* shell. It is relatively accessible experimentally and was studied by the experimental and theoretical tools available a generation ago. Recently, the opportunity presented itself to further explore this nucleus with a reaction favoring higher spins and using a modern full-sphere detector system. This has revealed a wealth of new results, as will be presented here, and provided challenges to theoretical understanding, especially of the still not well-characterized intruder structures.

Prior to the present work, the nuclear structure of ^{31}Si had been studied by β^- decay from ^{31}Al [1, 2], ^{30}Si(n,γ) thermal neutron capture [3–6], ^{30}Si(n,n) neutron resonances [7, 8], ^{29}Si(t,p) [9], ^{30}Si(t,d) [10, 11], ^{30}Si(d,p) [12–18] and ^{30}Si$(d,p\gamma)$ [19–22] particle transfer reactions. All the earlier experiments preferentially populated lower-spin states due to the nature of the reaction mechanisms with light projectiles.

Earlier studies of radiative decays in ^{31}Si were limited to the ^{30}Si(n,γ), lower energy ^{30}Si$(d,p\gamma)$, and β^- decay reactions. There were no γ-ray transitions observed to even the lowest negative-parity state at 3134 keV with spin and parity $J^\pi = \frac{7}{2}^-$. Prior to the present work, there have been several negative-parity states identified or suggested by the earlier (d,p) and neutron resonance studies [7, 8, 12–18]. The maximum spin assigned was $J^\pi = \frac{7}{2}^-$.

In this work, the ^{18}O(^{18}O, αn) fusion-evaporation reaction was employed to populate higher-spin states in ^{31}Si. Multiple γ coincidence events were detected by Gammasphere, an array of 101 Compton-suppressed high-purity Germanium detectors. The α particles were detected in coincidence in the Microball array for channel separation and kinematic correction of the recoil nuclei thereby resulting in a better Doppler correction.

II. EXPERIMENTAL PROCEDURE AND ANALYSIS METHOD

The 24-MeV ^{18}O beam was provided by the Argonne Tandem Linac Accelerator System (ATLAS) at Argonne National Laboratory, with typical beam currents of about 30 pnA. The 260 μg/cm^2 ^{18}O target was made at Florida State University by the electrolysis of water enriched to 97% in ^{18}O on a 12.7 μm tantalum backing. The thickness of the tantalum backing was specifically chosen such that the lighter evaporated particles (protons and α

particles) pass through the backing Ta layer with limited energy loss and reach the charged-particle detector, while the heavier beam particles are stopped.

Microball [23], a nearly 4π array of 95 CsI(Tl) scintillators, was used to detect and identify the light charged particles. Aside from particle identification, information about the energies and angles of the evaporated particles was extracted from Microball and subsequently utilized to perform event-by-event kinematic reconstruction of the ^{31}Si recoils resulting in better Doppler correction. The de-exciting γ rays from ^{31}Si were selected by a coincidence requirement with α particles and detected in Gammasphere [24].

III. RESULTS

Much of the γ-decay intensity observed in the present experiment flows through the 1695-keV $5/2_1^+ \rightarrow 3/2_1^+$ ground-state transition. The spectrum measured in coincidence with α particles and 1695-keV γ rays is presented in Fig. 1 to give an overall view of the data. The corresponding γ-ray spectrum in coincidence with α particles and the 1439-keV line highlights the decays to the lowest negative-parity state with spin-parity $7/2^-$ at 3134 keV as is shown in Fig. 2.

For clarity, the ^{31}Si level scheme from this analysis has been divided into two figures with the predominantly positive-parity states given in Fig. 3 and the predominantly negative-parity levels provided in Fig. 4 along with the lower positive-parity states to which they decay. This separation according to parity is based on previous information and on the parity of the states to which each level decays. Some individual cases will be discussed later. All the energy levels, observed decays, and intensities from the present work are listed in Table I.

The level scheme is based on previous work and on the γ lines newly observed here. All the transitions shown were observed in the present experiment to be in coincidence with α particles and with other γ lines. A quadruplet of γ lines near 2175 keV could only be partially separated by the various coincidence gates and this reduced somewhat the accuracy with which their energies and intensities could be determined, even though placements were well established. Two of these transitions are in cascade among the negative-parity states. More details on the experimental results can be found in [25].

Prior to the present work, the highest positive-parity spin previously assigned in ^{31}Si was

$5/2^+$ to the 1695- and 2788-keV states. An orbital angular momentum transfer value of $\ell = 4$ was assigned to the 3874-keV level in only one [16] of the (d, p) reactions. Although the possible spins consistent with $\ell = 4$ ($7/2^+$ and $9/2^+$) are shown in parentheses in the compilation of Ref. [26], likely because no other (d, p) experiment reported an ℓ value, the large number of newly discovered γ decays to this level, most of which come from unbound states, support the higher spin values consistent with $\ell = 4$. The present observation of a γ-decay branch from the 3874-keV level to the $3/2^+$ ground state rules out $9/2^+$, leaving $7/2^+$ as the possible spin-parity assignment. Interestingly, this indicates that the lowest $7/2^+$ level lies 740 keV above the lowest $7/2^-$ state. This is presumably due to the higher spin available from the $f_{7/2}$ intruder orbital.

Gamma decays were observed in the present work only to one state above the 3874-keV level in Fig. 3. This is the 4967-keV level, and all 3 decays into it come from unbound states which are likely to have relatively high spin or else their γ decays would not compete with neutron decay. No (d, p) ℓ transfer value has been reported for the 4967-keV state. Decay branches from it to two $5/2^+$ states and the newly assigned $7/2^+$ one were observed in the present work. These observations limit its maximum spin to $9/2^+$, which is in good agreement with shell model-calculations discussed below.

The 3 lowest negative-parity states were well established by (d, p) reactions, among others. A number of decays have been observed in the present work for the first time. They proceed towards the lowest of these states, the 3134-keV $7/2^-$ one. The parent states of these decays must have negative parity and reasonably high spins, most likely $7/2^-$ to $11/2^-$. Gamma decays have been observed into 3 of these parent states from neutron-unbound levels. The strongest decay sequence flows through the 5311-keV state, suggesting the highest spin, $11/2^-$, for it.

A state at 5281 keV was assigned $(1/2)^-$ in the NNDC compilation based on an $\ell = 1$ determination in the latest (d, p) measurement [18]. It has been seen following thermal neutron capture, suggesting very low spin indeed. Only the strongest decay branch, that to the 752-keV $1/2^+$ level, has been seen in the present experiment.

IV. DISCUSSION

The large amount of new experimental information on states and decays in ^{31}Si testifies to the power of modern full-sphere Compton-suppressed high-resolution γ and charged-particle detector arrays, but it also presents a challenge to theoretical understanding. Fortunately, theoretical tools have also improved significantly. The excitation energy of radiatively decaying states in ^{31}Si now extends to over 9.3 MeV, including 14 states unbound to neutron decay.

A. Shell-model calculations

The experimental states have been compared with shell-model calculations using several effective interactions in two different model spaces. The effective single-particle energies [27] calculated for these interactions in ^{31}Si are listed in Table II to give an overview. The universal *s-d* (USD) interaction was developed by fitting the properties of many positive-parity states in nuclei between $A = 17$ and $A = 39$ [28] and was very successful in predicting the properties of many states not included in the fit. With the accumulation of substantially more experimental information, new fits were made to structure in the *s-d* shell in the same spirit. These closely related interactions were called USDA and USDB [29] and generally provide somewhat better descriptions to the higher-lying and higher-spin states. All of these *s-d* interactions allow particles to move freely in the $0d_{5/2}$, $0d_{3/2}$, and $1s_{1/2}$ orbitals, but not to other orbitals. It can be seen from Table II that the effective single-particle energies are very similar between USD and newer USDA.

There must be an odd number of particles or holes outside the *s-d* shell to form negative-parity states. An early shell-model interaction to allow particles out of the $0p$ orbitals and/or into the $0f$-$1p$ shells was called WBP [30] and was adjusted to fit ^{20}F and ^{20}Na [31]. It was found [32, 33] that the negative-parity states predicted for ^{32,34}P using the WBP interaction were computed much too high in excitation energy. Accordingly, the single-particle energies of the $0f_{7/2}$ and $1p_{3/2}$orbitals were reduced by 1.8 and 0.5 MeV, respectively, relative the original WBP interaction. This modified interaction was called WBP-a in those papers (and in this one). The reduction was too much for ^{31}Si, so somewhat intermediate *f-p* single-particle energies were tried here and given the name WBP-b. Relative to WBP the

$0f_{7/2}$ single-particle energy was reduced by 1.4 MeV, that of the $1p_{1/2}$ orbital was raised by 0.4 MeV, and the $1p_{3/2}$ and $0f_{7/2}$ orbitals were left unchanged. We do not claim that such variations in the interaction represent an optimum situation, only that they give some indication of what might be needed for a future, better crafted, more universal interaction. The effects on the effective single-particle energies are shown in Table II. The original WBP interaction was used USD for the *s*-*d* shell part, so WBP-b was modernized a little by substituting the USDA interaction.

B. Positive-parity states

The nucleus ^{31}Si lies near the middle of the $1s0d$ shell so its lower structure would be expected to be based on pure *sd* configurations. Shell-model calculations using the original USD interaction [28] and the successor USDA and USDB ones [29] have been successful for other nuclei in the *sd* shell. The current expansion of the level scheme to higher energies and spins provides a valuable new test of these interactions.

Excitation energies predicted using the USDA interaction are given in Table III along with likely matches with positive-parity experimental states. Spin-parity assignments are determined well only for the lower states. For the higher levels, the matches are based on proximity in energy, consistent with all known experimental information, including (d,p) ℓ transfer values, spin limits from the γ decays, and the tendency of heavy-ion induced fusion-evaporation reactions to favor the population of yrast and near-yrast states. Suitable matches could not be found for 3 states at 5443, 5836, and 5856 keV. Although they decay only to positive-parity states, better correspondence was found with calculated negative-parity states, as discussed below. In fact, an $\ell = 3$ value had already been assigned to the 5443 keV state in a (d,p) reaction, implying negative parity for it. In this nucleus, it appears that γ decay to negative-parity states is a more reliable indicator of negative parity than the converse, because there are no negative-parity states below 3 MeV.

Although somewhat by construction, the agreement in energy is good for a total of 30 states over such a wide range of energies, from the ground state to above 9 MeV, with an rms deviation of only 143 keV. In fact, the rms deviation doesn't increase above that computed for the states below 5 MeV. The comparison with calculations using the USDB interaction is almost identical with an rms value of 152 keV. The rms value increases to 212 keV with

the older USD interaction which was not fitted to as many higher-energy states. Note that levels newly reported here were not known at the time of any of the USDx fits, so they are true predictions.

At the minimum, Table III demonstrates an existence theorem that the USDA calculations are capable of representing the nature of a wide range of states in ^{31}Si. They predict a sufficient number of states with the right spins to explain the data. Although 2p-2h configurations involving the higher-spin $0f_{7/2}$ orbital will account for higher-lying, higher-spin, positive-parity states, they do not appear to be required within the range explored here. Alternatively, the procedure of fitting the USDA interaction to higher states in other nuclei may reproduce the effects associated with small mixing with 2p-2h configurations.

Another test of the shell-model wavefunctions is the comparison with experimental single-neutron transfer spectroscopic factors measured in the ^{30}Si(d,p)^{31}Si reaction [26], as shown in Table IV. The comparison for the low-lying positive-parity states, for which spectroscopic factors have been reported, is good.

C. Negative-parity states

The negative-parity structure in ^{31}Si was known to start at 3134 keV. A comparison of experimental negative-parity states with those calculated in the shell model for 1p-1h configurations using the WBP, WBP-a, and WBP-b interactions can be found in Table V and Fig. 5. While the experimental spin-parity assignments are firm for the lower states, the matching of experimental and theoretical states at higher excitation energies is based on all the known experimental information and on agreement in excitation energy. Such comparisons demonstrate that good calculated candidates exist for the observed states. With these identifications, there is good agreement in energy with the WBP-b calculations.

The $0p$ shell was opened for these calculations for the center of mass correction, but the hole occupancies in the $0p$ shell rarely exceed 2%, indicating that all these states are fp particle states to a very good approximation. Occupancies of πfp orbitals only exceed 5% in a single case where they reached 10%; so all these states have predominantly neutron fp particle configurations. The occupancies of the neutron $f_{7/2}$, $p_{3/2}$, and $p_{1/2}$ orbitals are indicated for each theoretical state by color-coded lengths of the level energy lines in Fig. 5. Note that no $\nu f_{5/2}$ occupancies exceeded 5% in the WBPx calculations and are not shown

in the figure.

It is clear from Fig. 5 that most of the states calculated with the WBP interaction are computed to be an MeV or so too high, as mentioned above. Equally clear is that the single-particle energy reductions of WBP-a result in lowered calculated energies, about half an MeV below the experimental data. In spite of the variations in excitation energy, all the calculations indicate rather similar occupancies.

The WBP-b interaction gives the best description of the experimental data, but it was adjusted for the odd Si isotopes. Still, it leads to interesting insights into the structure of ^{31}Si, as well as into shell evolution. First, one can see that the lowest negative-parity state, $7/2^-$, is an almost pure $\nu f_{7/2}$ particle state in all the calculations, consistent with the relatively large spectroscopic factor observed in the (d,p) reaction [16]. Its excitation energy closely follows the position of the $\nu f_{7/2}$ single-particle energy in the interactions.

The next state, $3/2^-$, has predominantly a $\nu p_{3/2}$ particle configuration in all the calculations, consistent with its relatively large (d,p) spectroscopic factor. Its excitation energy agrees well with those calculated with WBP and WBP-b, but is predicted too low with WBP-a, the only version of the interaction with a lowered $\nu p_{3/2}$ single-particle energy.

Interestingly, the second $3/2^-$ level is predominantly of $\nu f_{7/2}$ particle character in all the calculations. The spin 2 $\hbar$ difference with respect to that of the intruder $f_{7/2}$ particle must come from a rearrangement of the remaining ^{30}Si sd particles from their minimum energy, zero-spin configuration in the two lowest negative-parity states. In fact, the largest change in sd occupancies occurs between these two $3/2^-$ states the second of which also has the largest πfp occupancy of 11%. The largest disagreement in energy between experiment and results from the WBP-b calculation occurs for the second $3/2^-$ state. Only the single-particle energy of the $\nu f_{7/2}$ orbital would change its excitation energy much, but such a change would spoil the agreement for all the higher-spin states. This disagreement can be regarded as a problem or as a challenge for future theory. The configuration of the third $3/2^-$ level is predominantly $\nu p_{3/2}$ like the first one and its predicted excitation energy is also about the same in all WBP variants, except WBP-a where the $\nu p_{3/2}$ orbital was lowered by 0.5 MeV.

Another interesting state is the first $1/2^-$ one. All the calculations imply a predominant $\nu 1p_{1/2}$ configuration. It is also unique because no other state in this region has more than 5% $\nu 1p_{1/2}$ occupancy. As such, this level provides an almost unique determination of the

position of the $\nu 1p_{1/2}$ orbital, at least for this nucleus. Since the $1p_{1/2}$ single-particle energy was not well determined in the original WBP interaction, it was raised by 400 keV in the WBP-b variant used here. This change was engineered to give excellent agreement with this lowest $1/2^-$ state and it barely affected the energies of the other levels. The calculations also show a 9% $0p$ hole contribution to the configuration of this state.

Single-neutron transfer spectroscopic factors provide another test of the shell-model wavefunctions. The comparison for the lower-lying negative-parity states is included in Table IV. The comparison with the lowest intruder state ($7/2^-$) is good, but the lower (higher) measured spectroscopic factor for the first (second) $3/2^-$ state compared to theory, may suggest that the configurations of the two lowest $3/2^-$ states are more mixed than the calculations with the WBP-b interaction predict. There is also reasonable agreement for the lowest $1/2^-$ and $5/2^-$ states.

It is informative to compare the excitation energies of the lowest intruder states as a function of neutron number N in the odd Si isotopes [34], as provided in Fig. 6. The excitation energies of all these states decrease with increasing N with the largest drop occurring when approaching the shell closure at $N = 19$ in ^{33}Si. A similar pattern was seen in the even-A P isotopes [33]. The WBP-b calculations, also shown in Fig. 6, qualitatively reproduce the decreasing trend in the lowest negative-parity states with increasing neutron number.

Taken together, it appears that the WBPx interactions reproduce the behavior of the 1p-1h negative-parity states as a function of neutron number better than its variation with proton number, for which the $\nu f_{7/2}$ and $\nu p_{3/2}$ single-particle energies require significant changes, at least between $Z = 14$ (Si) and $Z = 15$ (P) for the odd-N isotopes. This contrasts with the good description of the pure *sd* states using the USDx interactions and underlines the greater challenge presented by the *sd*-*fp* cross-shell excitations.

D. Unbound states

An R-matrix analysis of a neutron resonance experiment on ^{30}Si [8] lists 24 $\ell = 0$, 1, or 2 $\hbar$ resonances with J^π of $1/2^+$, $1/2^-$, $3/2^-$, $3/2^+$ and $5/2^+$ between incident neutron energies of 0.2 to 1400 keV (Ex = 6587 to 7945 keV) with neutron decay widths of 0.26 to 15 keV. Radiative decay could not compete with these keV size widths. In contrast, the

present heavy-ion fusion-evaporation reaction which favors higher-spin states has populated 14 γ decaying states from 6587 to 9323 keV with likely spins of $5/2^+$ to $15/2^-$. The latter states are indicated with red arrows in the neutron resonance graph of Fig. 7 which is taken from Ref. [8] . This figure indicates how these higher-spin states that decay radiatively are distributed among the lower-spin neutron resonances, but differ in energy except, possibly, for the present 6888-keV state and the $3/2^-$ resonance at 6880 keV with $\Gamma_n = 0.26$ keV. Although the energy difference is just outside our error estimate, these must be different states since γ decay could not compete with such a large neutron decay width. Also, a $3/2^-$ level is predicted nearby at 6759 keV in the WBP-b calculation. Such an intermingling among neutron and γ decaying states has been observed in a few other *sd* shell nuclei, including ^{19}O [35] and ^{27}Mg [36], where γ deexcitation was attributed to inhibition of neutron decay through a combination of angular momentum barriers and very low spectroscopic factors (S.F.).

To estimate the competition between the neutron and gamma decay modes from the unbound states, neutron decay widths assuming a unity S.F. for neutron emission to the ground state of ^{30}Si have been calculated using the square well estimate [37] with a channel radius of 4.2 fm [8] and compared with electromagnetic decay widths calculated for the observed transitions in the shell model using the USDA (positive-parity) or WBP-b (negative-parity) interactions. For comparison, another neutron decay width estimate using a Woods-Saxon-shaped barrier [38] was calculated. The results are found in Table VI. Since neutron decay has not been observed from these states, the maximum possible neutron-decay S.F. consistent with Γ_γ being at least equal to Γ_n, are listed in the last column of Table VI.

While the neutron penetrabilities and γ decay widths in Table VI have varying degrees of model dependence, the experimental fact remains that substantial (probably dominant) γ decays have been observed from the states in Table VI, while neutron formation and decay have not been observed in a sensitive experiment[8] . In many cases it appears that the angular momentum barrier is not sufficient to retard the neutron decay sufficiently to explain the observed predominant radiative decay. It is hard to escape the conclusion that neutron decay must be inhibited further by S.F. values in the range of 10^{-2} to 10^{-4} or less. This is consistent with previous observations [35, 36]. As a test of these estimates, the neutron decay spectroscopic factor for the 6661 keV state was calculated in the shell model to be 0.0012, a factor of 2 above the upper limit in Table VI. However, shell model calculations

are not reliable for calculating small transition strengths which are very sensitive to small components in the wave functions and cancellations between them. Basically, both values say that the S.F. is very low and no further conclusion about agreement or disagreement can be drawn.

The positions of these low-spin neutron resonant states provide another test of the shell model calculations. Good candidates can be found for the $\ell = 0$ and $\ell = 2$ resonances reported in Ref. [8] among the states calculated in the *sd* shell model using the USDA interaction. These resonances are shown in Table III in square brackets. There is almost a one-to-one correspondence in the number of predicted and observed levels. The rms deviation is only 106 keV, based on the identifications shown. A similar test for the $\ell = 1$ resonances with the WBP-b calculations is found in Table VII. All the calculated and reported $1/2^-$ and $3/2^-$ states are given in the Table. There are good matches for all the reported $3/2^-$ states with the WBP-b predictions with one additional predicted level. The latter state could have been missed in the R-matrix analysis of Ref. [8]. Nine $1/2^-$ resonances were reported in this energy range, but the WBP-b calculations predict only 5 at most, with good energy matches for 3. This is the only case seen of either an excess of experimental states or a lack of theoretical ones. It could possibly represent some ambiguities in the R-matrix analysis for broad resonances or a problem in the shell-model predictions.

V. SUMMARY

The nucleus ^{31}Si was formed in the ^{18}O(^{18}O, αn) fusion-evaporation reaction using a 24-MeV ^{18}O beam from ATLAS on a 260 μg/cm^2 ^{18}O target. Evaporated α particles from the reaction were detected and identified in the Microball detector array for channel selection. Multiple γ-ray coincidence events were detected with Gammasphere. The energy and angle information on the decay α particles was used to determine the ^{31}Si recoil kinematics on an event-by-event basis for accurate Doppler correction. A wealth of new information on the level and decay scheme of ^{31}Si was deduced.

The energies of the positive-parity states up to 9323 keV were reproduced well by shell-model calculations using the USDA interaction assuming an inert ^{16}O core and no particles in the fp shell. Although spin assignments are not firm for the higher-lying states, the calculations indicate that there are, at least, shell-model levels with excitation energies near

the experimental ones, fitting all the constraints imposed by the data and giving an excellent rms deviation of about 150 keV for 29 states.

A bigger challenge is understanding the structure of the negative-parity states which must involve an odd number of particles outside the *sd* shell. Several versions of the WBP interaction were compared with experiment. All gave similar results for the structure of the states and their relative spacings. They differed mainly on the overall shift of the 1p-1h negative-parity states compared to the 0p-0h positive-parity ones. The best agreement came from a WBP variant (called the WBP-b interaction) in which the $0f_{7/2}$ single-particle energy was lowered 1.4 MeV below that in the WBP interaction which was optimized around $A \approx 20$ in contrast to WBP-a, where it was lowered 1.8 MeV to best fit the even P isotopes. The structures of most of the negative-parity states are dominated by configurations with one neutron in the $0f_{7/2}$ orbital. A few low-spin states have primarily a neutron in the $1p_{3/2}$ orbital, and the structure of the lowest $1/2^-$ state involves primarily a neutron in the $1p_{1/2}$ orbital.

The *sd-pf* shell-model calculations using the WBP-b interaction reproduce the energies of the experimental negative-parity states with established spin assignments rather well and provide good candidates for the others. However, this agreement comes at the price of adjusting some *fp* single-particle energies relative to the original WBP interaction and to that which best fitted ^{32,34}P. Such changes point to the need for a more comprehensive fit of negative-parity states over the whole range of nuclei in the *sd* shell. This would require large-scale computing capability and is well beyond the scope of the present work. However, the negative-parity states observed in this and many other recent investigations provide the raw materials for such a computational project.

Another interesting aspect of these ^{31}Si results is the discovery of radiative decays from 14 states located above the neutron binding energy, despite the fact that strong-interaction neutron decay is not impeded by a Coulomb barrier and is usually orders of magnitude faster than electromagnetic decay. Only large angular momentum barriers and/or very small n + ^{30}Si spectroscopic factors can hinder neutron decay to the extent that it does not compete with γ rates. Both factors appear critical to the observations in ^{31}Si. An older neutron resonance experiment demonstrates that the lower-spin states in the same unbound energy range do decay primarily by neutron emission. Interestingly, there are good candidates in the shell-model calculations to match the energies of both the higher-spin γ and low-spin n

decaying states, with the possible exception of a few unbound $1/2^-$ resonances which may be the most difficult to determine experimentally due to their large widths.

ACKNOWLEDGMENTS

This work was supported by U.S. National Science Foundation under grant NSF 14-01574 and the U.S. Department of Energy, Office of Science, Office of Nuclear Physics under Grants No. DE-SC0009883 (FSU), DE-AC02-05CH-11231 (LBNL), DE-AC02-06CH-11357 (ANL), and DE-FG02-88ER-40406 (W.U.). This research uses resources of ANL's ATLAS facility, which is a DOE Office of Science user facility.

---

[1] D. R. Goosman and D. E. Alburger, Phys. Rev. C, **7**, 2409 (1973).

[2] C. Détraz, D. Guillemaud, G. Huber, R. Klapisch, M. Langevin, F. Naulin, C. Thibault, L. C. Carraz, and F. Touchard, Phys. Rev. C, **19**, 164 (1979).

[3] G. Beard and G. Thomas, Nuclear Physics A, **157**, 520 (1970).

[4] A. Spits, A. O. D. Kamp, and H. Gruppelaar, Nuclear Physics A, **145**, 449 (1970).

[5] M. A. Islam, T. J. Kennett, and W. V. Prestwich, Phys. Rev. C, **41**, 1272 (1990).

[6] S. Raman, E. T. Jurney, J. W. Starner, and J. E. Lynn, Phys. Rev. C, **46**, 972 (1992).

[7] J. Boldeman, B. Allen, A. de L. Musgrove, and R. Macklin, Nuclear Physics A, **252**, 62 (1975).

[8] J. A. Harvey, W. M. Good, R. F. Carlton, B. Castel, J. B. McGrory, and S. F. Mughabghab, Phys. Rev. C, **28**, 24 (1983).

[9] R. Middleton and D. Pullen, Nuclear Physics, **51**, 77 (1964).

[10] J. Hanspal, K. Pearce, N. Clarke, R. Griffiths, R. E. Brown, R. Hardekopf, and W. Grebler, Nuclear Physics A, **455**, 494 (1986).

[11] K. Pearce, N. Clarke, R. Griffiths, P. Simmonds, D. Barker, J. England, M. Mannion, and C. Ogilvie, Nuclear Physics A, **467**, 215 (1987).

[12] C. Browne and J. Radzyminski, Nuclear Physics, **19**, 164 (1960).

[13] M. Betigeri, R. Bock, H. H. Duhm, S. Martin, and R. Stock, Zeitschrift für Naturforschung, **21**, 980 (1966).

[14] B. Wildenthal and P. Glaudemans, Nuclear Physics A, **108**, 49 (1968).

[15] G. W. Hoffmann, J. McIntyre, and W. R. Coker, Phys. Rev. C, **10**, 1671 (1974).

[16] D. L. Watson and D. N. Slater, Journal of Physics G: Nuclear Physics, **9**, 1417 (1983).

[17] N. Davis and J. Nelson, Nuclear Physics A, **468**, 357 (1987).

[18] Š. Piskoř, J. Novák, E. Šimečková, J. Cejpek, V. Kroha, J. Dobeš, and P. Navrátil, Nuclear Physics A, **662**, 112 (2000).

[19] R. Gill, G. Littlewood, J. Lopes, and H. Rose, Nuclear Physics A, **114**, 416 (1968).

[20] V. H. Webb, N. R. Roberson, R. V. Poore, and D. R. Tilley, Phys. Rev., **170**, 979 (1968).

[21] H. Graber, P. Glaudemans, and P. Endt, Nuclear Physics A, **149**, 1 (1970).

[22] M. J. Wozniak and D. J. Donahue, Phys. Rev. C, **1**, 601 (1970).

[23] D. Sarantites, P.-F. Hua, M. Devlin, L. Sobotka, J. Elson, J. Hood, D. LaFosse, J. Sarantites, and M. Maier, Nuclear Instruments and Methods in Physics Research Section A: Accelerators, Spectrometers, Detectors and Associated Equipment, **381**, 418 (1996).

[24] I.-Y. Lee, Nuclear Physics A, **520**, c641 (1990), nuclear Structure in the Nineties.

[25] P.-L. Tai, *A Gamma-ray Spectroscopy Study for Higher Spin Structure of 31Si*, Ph.D. thesis, Florida State University (2016), unpublished.

[26] NNDC, "National nuclear data center," Http://www.nndc.bnl.gov/.

[27] V. Zelevinsky and A. Volya, "Self-consistent field," in *Physics of Atomic Nuclei* (Wiley-VCH Verlag GmbH and Co. KGaA, 2017) pp. 391–420, ISBN 9783527693610.

[28] B. Wildenthal, Progress in Particle and Nuclear Physics, **11**, 5 (1984).

[29] B. A. Brown and W. A. Richter, Phys. Rev. C, **74**, 034315 (2006).

[30] E. K. Warburton and B. A. Brown, Phys. Rev. C, **46**, 923 (1992).

[31] E. K. Warburton, J. A. Becker, and B. A. Brown, Phys. Rev. C, **41**, 1147 (1990).

[32] P. C. Bender, C. R. Hoffman, M. Wiedeking, J. M. Allmond, L. A. Bernstein, J. T. Burke, D. L. Bleuel, R. M. Clark, P. Fallon, B. L. Goldblum, T. A. Hinners, H. B. Jeppesen, S. Lee, I.-Y. Lee, S. R. Lesher, A. O. Macchiavelli, M. A. McMahan, D. Morris, M. Perry, L. Phair, N. D. Scielzo, S. L. Tabor, V. Tripathi, and A. Volya, Phys. Rev. C, **80**, 014302 (2009).

[33] P. C. Bender, S. L. Tabor, V. Tripathi, C. R. Hoffman, L. Hamilton, A. Volya, R. M. Clark, P. Fallon, A. O. Macchiavelli, S. Paschalis, M. Petri, M. P. Carpenter, R. V. F. Janssens, T. Lauritsen, E. A. McCutchan, D. Seweryniak, S. Zhu, C. J. Chiara, X. Chen, W. Reviol, D. G. Sarantites, and Y. Toh, Phys. Rev. C, **85**, 044305 (2012).

[34] Z. M. Wang, R. Chapman, X. Liang, F. Haas, M. Bouhelal, F. Azaiez, B. R. Behera, M. Burns, E. Caurier, L. Corradi, D. Curien, A. N. Deacon, Z. Dombradi, E. Farnea, E. Fioretto, A. Gadea, A. Hodsdon, F. Ibrahim, A. Jungclaus, K. K. Keyes, V. Kumar, A. Latina, N. Margineau, G. Montagnoli, D. R. Napoli, F. Nowacki, J. Ollier, D. O'Donnell, A. Papenberg, G. Pollarolo, M.-D. Salsac, F. Scarlassara, J. F. Smith, K. M. Spohr, M. Stanoiu, A. M. Stefanni, S. Szilner, M. Trotta, and D. Verney, Phys. Rev. C, 064301 (2010).

[35] R. Dungan, S. L. Tabor, V. Tripathi, A. Volya, K. Kravvaris, B. Abromeit, D. D. Caussyn, S. Morrow, J. J. I. Parker, P.-L. Tai, and J. M. VonMoss, Phys. Rev. C, **93**, 021302 (2016).

[36] R. Dungan, S. L. Tabor, R. S. Lubna, A. Volya, V. Tripathi, B. Abromeit, D. D. Caussyn, K. Kravvaris, and P.-L. Tai, Phys. Rev. C, **94**, 064305 (2016).

[37] A. Volya, "http://nucracker.volya.net,".

[38] N. Schwierz, I. Wiedenhover, and A. Volya, arXiv, **0709.3525**.

TABLE I: **Energies, relative intensities, and placement of γ transitions observed in the present work.**

E_x (keV)	J^π	E_γ (keV)	I_γ
752.2(2)	$1/2^+$	752.2(2)	15.6(8)
1694.9(3)	$5/2^+$	942.6(4)	1.2(4)
		1695.0(3)	100
2316.9(22)	$3/2^+$	621.5(15)	0.3(2)
		1564.6(20)	0.4(2)
		2315.7(20)	1.8(3)
2788.0(15)	$5/2^+$	(1093)	
		2037.7(30)	0.5(2)
		2788.3(12)	17(3)
3133.5(7)	$7/2^-$	345.3(5)	0.4 (1)
		1438.5(3)	70(3)
3532.9(17)	$3/2^-$	2780.0(15)	6.0 (25)
3874.0(17)	$7/2^+$	1086.0(20)	< 0.1
		2179.2(15)	6.6(5)
		3874.2(15)	6.4(5)
4261.0(17)	$(3/2^+)$	3508.6(15)	0.8(2)
4382.4(22)	$3/2^-$	3629.8(20)	1.9(2)
4717(2)	$1/2^+$	3964(2)	0.9(1)
4943(3)	$(7/2^+)$	2155(2)	1.9(2)
		3249(3)	2.1(2)
4967(2)	$(9/2^+)$	1093.7(8)	3.5(3)
		2180(2)	3.8(20)
		3274(3)	1.3(3)
4999(2)		1864.1(15)	10.5(10)
		1124.2(15)	1.4(5)
5279(3)	$(1/2)^-$	4526.4(20)	1.5(5)
5311(2)		2177.9(15)	16(4)
5443(2)		2654.6(15)	3.2(5)
		3126.0(25)	< 0.5
5451(3)		3756(3)	1.1(4)
5600(3)		3905(2)	0.6(4)
5612(2)		2478.0(15)	6.2(8)
5656(2)		3961(2)	1.1(4)
5677(2)		2888.7(15)	2.6(5)
5791(3)		3003(2)	1.5(2)
5836(3)		4141.2(25)	3.9(4)
5856(4)		3539(3)	< 0.5
5985(3)		2111(2)	0.8(3)
		4287(4)	1.3(3)
6250(2)		4555(2)	0.9(2)
6422(3)		2548.0(25)	0.7(3)

Continued on next page

TABLE I – continued from previous page

E_x (keV)	J^π	E_γ (keV)	I_γ
		4718(3)	0.3(1)
6473(5)		4156(4)	< 0.5
6584(3)		3796(3)	0.3(2)
		4889(3)	0.8(2)
6661(2)		2787.7(35)	0.6(3)
		3873.7(22)	0.3(2)
		4966.2(22)	1.5(3)
6794(2)		1796.2(10)	0.6(5)
		3658(2)	1.5(10)
6888(4)		5189(4)	0.5(2)
		3016(4)	0.7(4)
7033(3)		2066.4(15)	< 0.8
7111(4)		4794(3)	< 0.5
7226(2)		1615.0(12)	1.1(7)
		4091(3)	0.5(3)
7484(3)		2173(2)	2.8(15)
7544(3)		4756(3)	0.2(1)
7582(3)		3708(23)	0.5(3)
8359(3)		3048(2)	0.8(5)
8389(4)		4515(4)	0.4(3)
8926(3)		3615(2)	1.5(10)
9216(4)		4249(3)	< 0.5
9323(4)		4356(3)	< 0.5

TABLE II. Effective single-particle energies for ^{31}Si from the shell-model interactions discussed in this paper.

Orbital	WBP-b	WBP-a	WBP	USDA	USD
$0s_{1/2}$	-39.96	-39.96	-39.96		
$0p_{3/2}$	-29.10	-29.12	-29.12		
$0p_{1/2}$	-24.33	-24.36	-24.36		
0d5/2	-16.56	-16.43	-16.43	-16.56	-16.43
0d3/2	-9.562	-9.553	-9.553	-9.561	-9.552
1s1/2	-11.52	-11.76	-11.76	-11.52	-11.76
0f7/2	-2.686	-3.097	-1.297		
0f5/2	3.448	3.440	3.440		
1p3/2	-2.38	-2.925	-2.425		
1p1/2	-0.813	-1.219	-1.219		

TABLE III: An assignment of likely positive-parity experimental states (listed as energies in keV) to states predicted in the shell model using the USDA interaction. These suggested correspondences are consistent with the γ-decay patterns, but should be considered as model-dependent assignments. Only states with J $\geq$ 7/2 are listed above 8100 keV. Experimental energies in square brackets are from the neutron resonance measurement [8].

2J	USDA	Exp.	Diff.	2J	USDA	Exp.	Diff.
3	0	0	0	5	7012		
1	553	752	199	3	7160	[7211]	[51]
5	1604	1695	91	7	7184	7111	[-73]
3	2186	2317	131	3	7249	[7269]	[20]
5	2611	2788	177	5	7336		
7	3894	3874	-20	11	7377	7033	-344
3	4142	4261	119	9	7446	7582	136
1	4524	4717	193	7	7450		
7	4755	4943	188	1	7564	[7731]	[167]
9	4830	4967	137	3	7599	[7438]	[-161]
3	5055			7	7613	7544	-69
5	5219	5451	232	5	7722	[7766]	[71]
3	5344			9	7806		
5	5367	5600	233	1	7889		
7	5683	5656	-27	3	7942	[7847]	[-95]
5	5714	5677	-37	3	8083	[7943]	[-140]
9	5727	5791	64	7	8101		
7	6114	6250	136	11	8243	8389	146
9	6167	5985	-182	7	8286		
3	6278			7	8364		

Continued on next page

TABLE III – continued from previous page

2J	USDA	Exp.	Diff.	2J	USDA	Exp.	Diff.
1	6289			9	8519		
1	6464			11	8642		
3	6466	6473	7	7	8683		
9	6468	6422	-46	11	8794		
5	6487			9	8934		
7	6550	6584	34	7	9053		
5	6651	6661	10	13	9062	9216	154
7	6711	6888	179	7	9188		
3	6831	[6815]	[-16]	9	9279		
1	6862	[6763]	[-99]	11	9289	9323	34

TABLE IV. A comparison of measured single-neutron spectroscopic factors from the ^{30}Si(d,p)^{31}Si reaction [26] with those calculated in the shell model using the USDA (WBP-b) interaction for the positive- (negative-)parity states.

Ex(keV)	$2J^\pi$	C^2S(Exp.)	C^2S(S.M.)
0	3^+	2.8	2.2
752	1^+	0.51	0.50
1695	5^+	< 0.1	0.07
2317	3^+	0.16	0.14
2788	5^+	0.26	0.35
3134	7^-	4.8	5.6
3533	3^-	1.6	2.9
4382	3^-	0.55	0.08
5279	1^-	0.89	1.3
5443	5^-	0.59	0.26

TABLE V. An assignment of likely negative-parity experimental states (listed as energies in keV) to states predicted in the shell model using 3 variations of the WBP cross-shell interaction. Spins of the first 4 experimental states are established experimentally. The correspondences of shell-model states with higher-lying experimental levels are consistent with their γ decays and other measured properties, but must be considered shell-model assignments.

2J	WBP	WBP-a	WBP-b	Exp.
7	4112	2455	2922	3134
3	3580	2955	3524	3533
3	5931	4373	4747	4382
5	5556	4685	5075	
9	6342	4658	5121	4998
7	5818	4697	5231	
1	5006	4805	5264	5279
11	6706	5006	5375	5311
5	6241	4943	5479	5443
3	5795	5239	5743	5856
1	6064	5498	5801	
7	6294	5336	5754	5612
5	6754	5795	6042	5836
7	7330	5918	6110	
9		5894	6161	
11		6168	6667	6794
11			7493	7226
13			7540	7484
11			8563	8359
15			8784	8926

TABLE VI. Estimated decay widths for the neutron unbound states in ^{31}Si observed to decay by γ emission. The column labeled ℓ shows the minimum neutron decay orbital angular momentum for decay given the J^π shown in the previous column. Two different estimates of neutron decay width are shown to give an idea of the uncertainty: the barrier penetrability using a Woods-Saxon potential [ref] (square-well barrier) is listed in the column labeled WS (SW). Gamma-decay widths calculated from the shell model based on the identifications in Tables III and V in units of eV for calculation of the neutron spectroscopic factors and milli-Weisskopf units (mWU) for convenience of the reader. S.F. is the upper limit on the neutron-decay spectroscopic factor consistent with the observation of dominant radiative decay from these states. The highest limit comes from the square-well barrier. The Woods-Saxon barrier would give about a factor of 5 lower upper limit.

E_x (keV)	J^π	ℓ ($\hbar$)	E_n (keV)	WS(eV)	SW(eV)	Γ_γ (eV)	Γ_γ (mWU)	S.F.
6661	$5/2^+$	2	76	475	290	0.2	80	$< 6.9 \times 10^{-4}$
6794	$11/2^-$	5	214	1.0×10^{-3}	2.6×10^{-4}	0.021	6900	< 1
6888	$7/2^+$	4	311	1.5	0.62	0.11	40	< 0.18
7033	$11/2^+$	6	461	2.2×10^{-4}	5.5×10^{-5}	5.0×10^{-4}	3	< 1
7111	$7/2^+$	4	541	17	7.3	1.9×10^{-3}	160	$< 2.6 \times 10^{-4}$
7226	$11/2^-$	5	660	0.48	0.12	2.7×10^{-5}	530	2.2×10^{-4}
7484	$13/2^-$	7	927	1.2×10^{-4}	2.2×10^{-5}	5.1×10^{-3}	12	< 1
7544	$7/2^+$	4	989	240	120	0.014	6	$< 1.4 \times 10^{-4}$
7582	$9/2^+$	4	1028	350	120	0.035	16	$< 2.8 \times 10^{-4}$
8359	$11/2^-$	5	1831	110	30	6.5×10^{-3}	11	< 0.24
8389	$11/2^+$	6	1862	1.7	0.43	0.063	7200	$< 1.5 \times 10^{-3}$
8926	$15/2^-$	7	2417	0.18	0.03	5.6×10^{-3}	1900	< 1
9216	$13/2^+$	6	2717	27	4.7	0.018	2800	$< 3.8 \times 10^{-3}$
9323	$11/2^+$	6	2827	26	6.1	8×10^{-3}	5	$< 1.3 \times 10^{-3}$

TABLE VII. An assignment of measured $\ell = 1$ neutron resonances on a ^{30}Si target [8] with states predicted in the shell model using the WBP-b interaction. All predicted and measured $1/2^-$ and $3/2^-$ states within this energy range are listed.

2J	WBP-b	Exp.	Diff.
3	6759	6880	-121
1	6867	6592	275
1	7002	6987	15
3	7060		
3	7258	7308	-50
1	7404	7358	46
1		7368	
1		7372	
3	7556	7404	152
1		7535	
1		7821	
3	7729	7855	-126
3	7786	7899	-113
3	7930	7954	-24
1	7964	7882	82
3	8142		
1	8189	7926	263

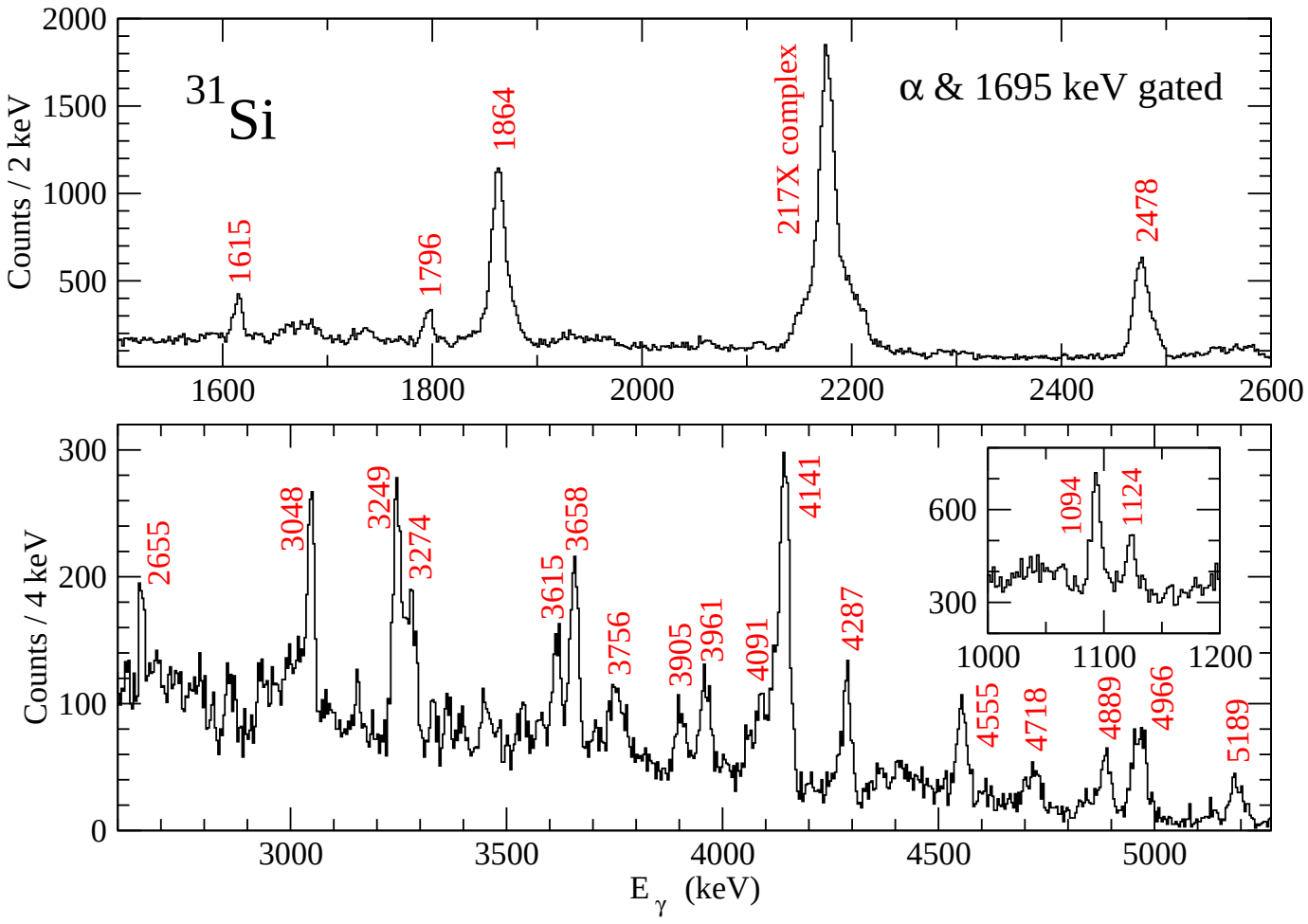

FIG. 1. Portions of the γ spectra in coincidence with α particles and 1695-keV γ rays. All of the γ lines in these regions are labeled with their energies in red color to indicate that they are newly reported.

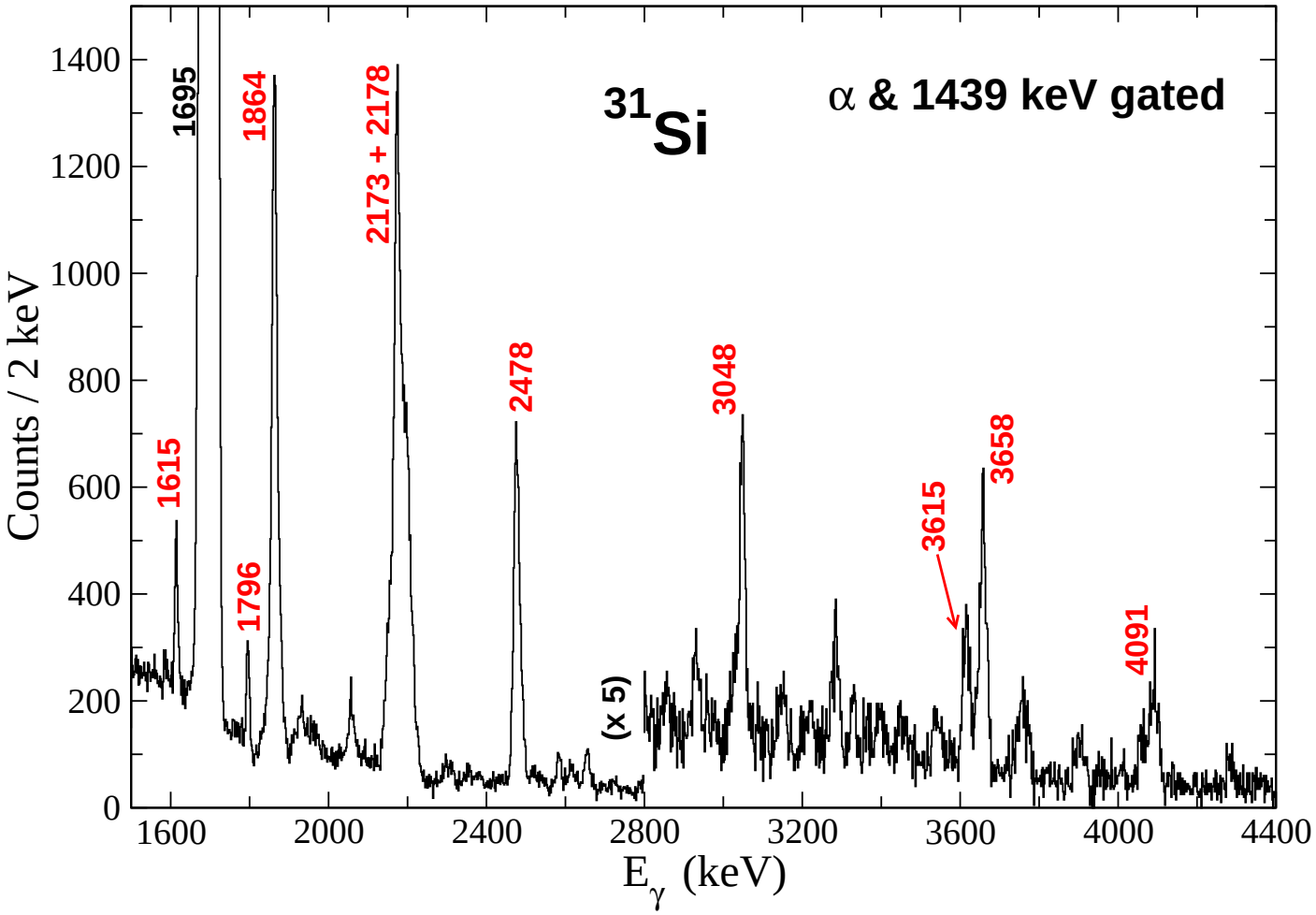

FIG. 2. Portions of the γ spectra in coincidence with α particles and 1439-keV γ rays. All of the γ lines in these regions are labeled with their energies in red color to indicate that they are newly reported.

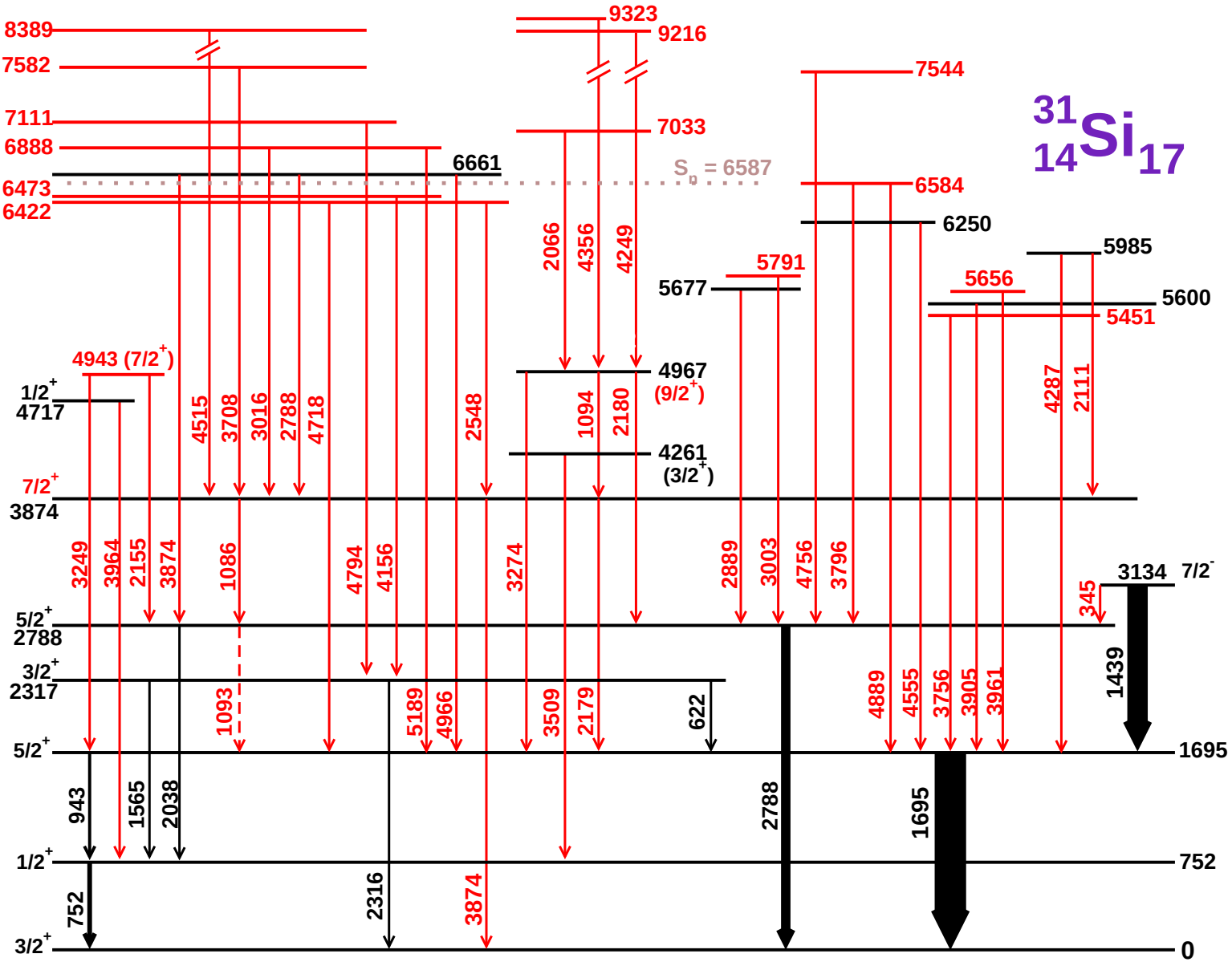

FIG. 3. Energy level scheme of likely positive-parity states in ^{31}Si from this work. The newly observed states and transitions are shown in red and the widths of the decay lines are proportional to their intensities.

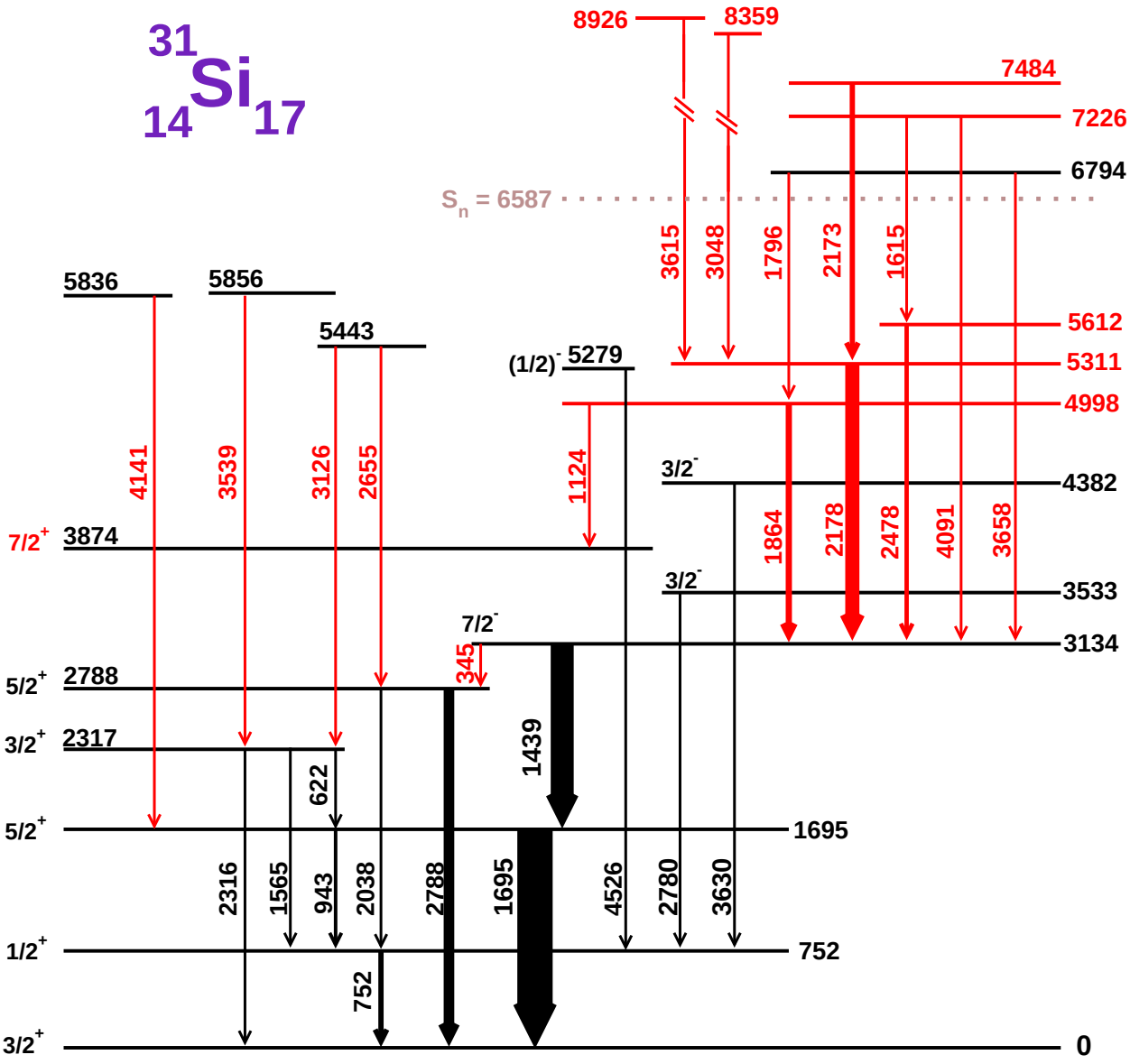

FIG. 4. Energy level scheme of likely negative-parity states in ^{31}Si from this work. See the caption of Fig. 3 for more information.

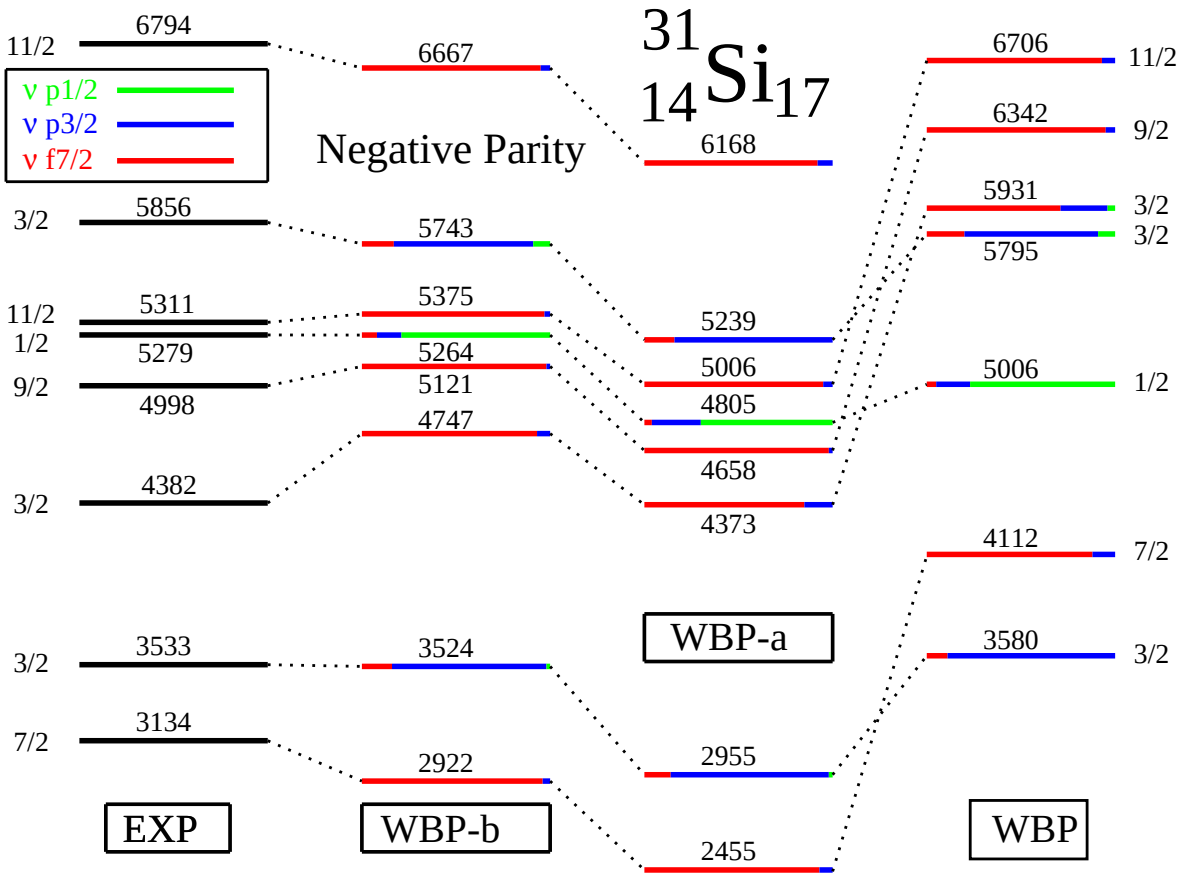

FIG. 5. A comparison of selected negative-parity experimental states with 1p1h states calculated with 3 versions of the WBP interaction. The theory level lines are color coded by the calculated occupancies of the neutron $0f_{7/2}$, $1p_{3/2}$, and $1p_{1/2}$ orbitals.

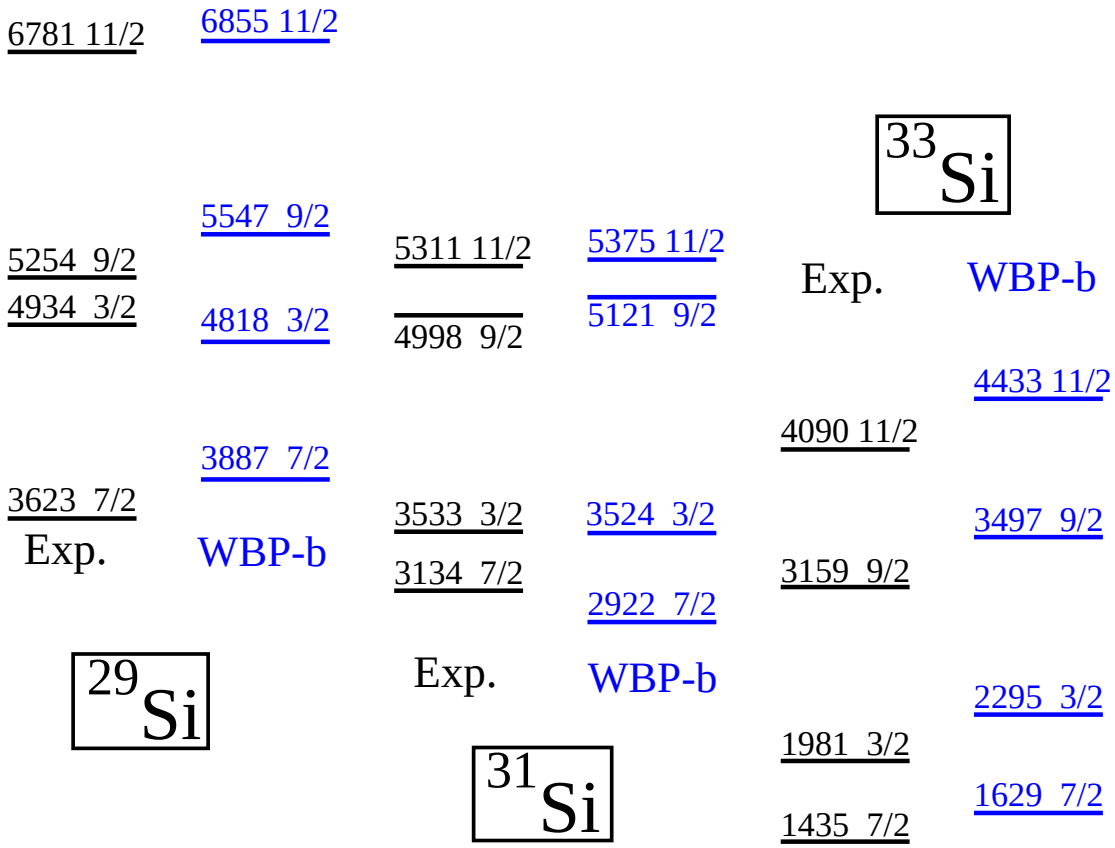

FIG. 6. A comparison of experimental energies of the lowest negative-parity states in ^{29,31,33}Si along with the calculated positions using the WBP-b interaction.

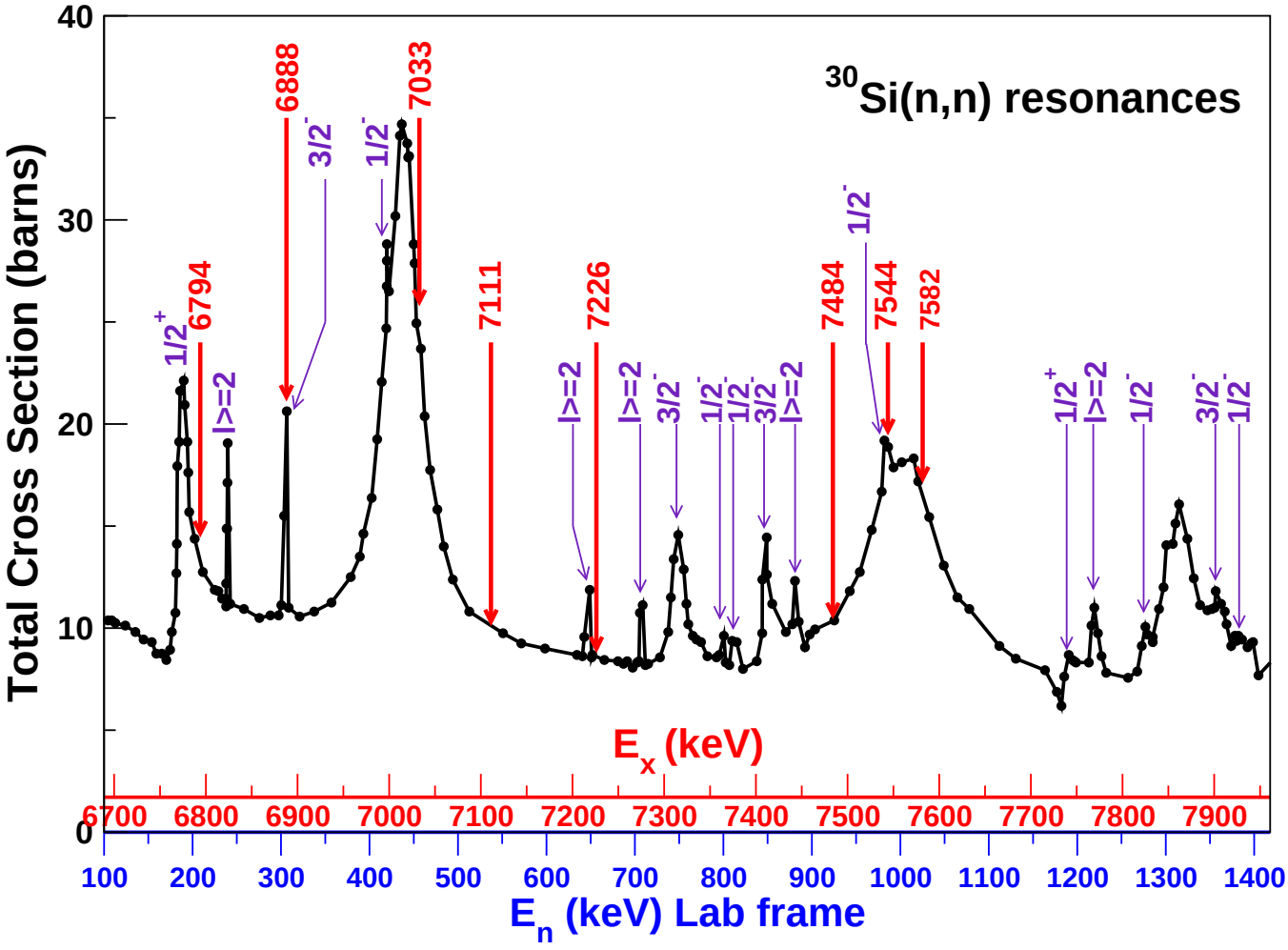

FIG. 7. Graph of neutron resonances on ^{30}Si from Ref. [8] with locations of the states seen in the present experiment indicated by vertical arrows. The 6888 keV state observed in the present work is not likely to be the the $3/2^-$ one reported in the n resonance experiment, as discussed in the text.